J. Phys. B: At. Mol. Opt. Phys. 26 (1993) 2429–2441. Printed in the UK

Electron impact excitation cross sections for CO

Lesley A Morgan† and Jonathan Tennyson‡

† Computer Centre, Royal Holloway, University of London, Egham, Surrey TW20 0EX, UK
‡ Department of Physics and Astronomy, University College London, London WC1E 6BT, UK

Received 25 March 1993, in final form 7 June 1993

Abstract. The R-matrix method has been used to calculate electron impact excitation cross sections for the lowest seven electronically excited states of CO in the energy range 6–18 eV. These states are represented using configuration interaction (CI) expansions and an algorithm for treating long CI expansions in scattering calculations is presented. The calculations are carried out for a range of internuclear distances $1.8 \leqslant R \leqslant 3.0\ a_0$. Several new resonance structures are identified. Good agreement is obtained with the recent experimental results of Furlong and Newell for the excitation of the a $^3\Pi$ state.

1. Introduction

Ab initio calculations for the electronic excitation of molecules are still remarkably few in number and until quite recently were restricted to two-state approximations. The R-matrix method (Gillan *et al* 1987, Morgan 1990) can, in principle, handle large numbers of target states and multistate calculations have been reported for H_2 (Branchett *et al* 1990), HeH^+ (Sarpal *et al* 1991), N_2 (Gillan *et al* 1990) and O_2 (Noble and Burke 1992). In practice, the number of states included is usually restricted by the availability of wavefunctions describing the more highly excited states of the target. An extension of the R-matrix method, which includes a non-adiabatic treatment of nuclear vibration, has also been used recently to calculate low energy vibrational excitation cross sections for a number of diatomics including CO (Morgan 1991).

Electron-impact excitation cross sections are required for a variety of applications. These include the modelling of plasmas, discharge pumped lasers, molecules adsorbed on to surfaces and various astrophysical applications, see, for example, McDaniel and Nigham (1982), Land (1978) and Urban (1991).

There has been little previous theoretical work on CO and, to our knowledge, only one which goes beyond two-state models. The results described here have been obtained using CI target wavefunctions in an eight-state model (the lowest eight states of CO, X $^1\Sigma^+$, a $^3\Pi$, a′ $^3\Sigma^+$, d $^3\Delta$, A $^1\Pi$, e $^3\Sigma^-$, I $^1\Sigma^-$, D $^1\Delta$, see figure 1) and cover the scattered electron energy range 6–18 eV. The recent work by Sun *et al* (1992) includes the same eight states as the present work but not necessarily all eight are included in a given calculation. They use the Schwinger multichannel variational method at a single fixed geometry and use single configuration representations of the target wavefunctions. Two of the more recent two-state calculations are those of Lee and McKoy (1982) and Weatherford and Huo (1990). The former have carried out a series of distorted wave calculations for the excitation of the A $^1\Pi$, a $^3\Pi$, a′ $^3\Sigma^+$, D $^1\Delta$ and d $^3\Delta$ states for electron energies in the 20–50 eV range. The latter have used the Schwinger multichannel method to calculate excitation cross sections for the

0953-4075/93/152429+13$07.50

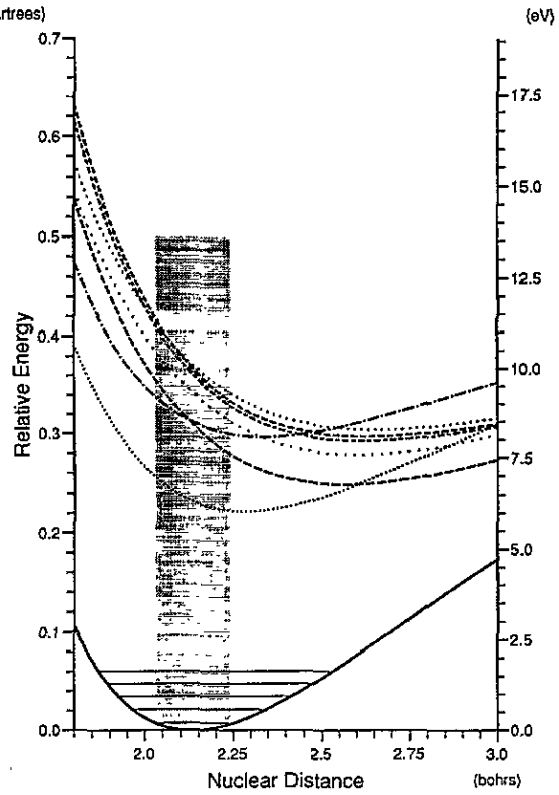

Figure 1. Potential energy curves. Full curve, CO X $^1\Sigma^+$ ground state; lowest dotted curve, a $^3\Pi$; long-broken curve, a' $^3\Sigma^+$; chain curve, A $^1\Pi$; other curves, in order of increasing energy, d $^3\Delta$, e $^3\Sigma^-$, I $^1\Sigma^-$, D $^1\Delta$; shaded rectangle, Franck–Condon region for ground vibrational level.

(Rydberg) b $^3\Sigma^+$ state. Neither calculation can therefore be compared directly with the present work.

There has been rather more experimental work in this area. This includes measurements by Mazeau *et al* (1972), Wells *et al* (1973), Swanson *et al* (1975), Newman *et al* (1983), Mason and Newell (1988) and Allan (1989). Although all observe structures in the cross sections, there is no overall consensus as to their origins. More measurements are currently in progress at Kaiserslautern and University College London.

2. Method

We carried out a sequence of fixed nuclei calculations for four overall symmetries and a range of internuclear separations using the multicentre R-matrix method (see Gillan *et al* 1987 for full details).

The trial wavefunctions used at each internuclear separation R have the form

$$\psi_k = \sum_{ij} \phi_i(x_1 \ldots x_N) u_{ij}(x_{N+1}) a_{ijk} + \sum_i \chi_i(x_1 \ldots x_{N+1}) b_{ik} \qquad (1)$$

where ϕ_i are target CI wavefunctions and the $u_{ij}(x)$ are numerical continuum orbitals. In the present calculations spherical Bessel functions were found to be adequate for the latter and angular momenta up to $l = 6$ were used. The χ_i are two-centre quadratically integrable functions constructed from the target occupied and virtual molecular orbitals, which are, in turn, expanded as a linear combination of STOs.

In order to model excited states, CI target wavefunctions are clearly desirable. Computational considerations have restricted previous R-matrix scattering calculations for the electronic excitation of diatomics to CI target wavefunctions of less than 30 configurations. Calculations at this level for CO were found to be both computationally very demanding and not accurate enough for present purposes. In this context it should be noted that the lower symmetry of CO means that both target configuration lists and the number of continuum functions are approximately doubled for a calculation of equivalent accuracy on a homonuclear diatomic such as N_2.

To help break the bottleneck in the calculation, which is caused by the generation of symbolic matrix elements, we have adapted the 'prototype CI method' of Liu and coworkers (Liu and Yoshimine 1981, Liu and Lengsfield 1991) to the special case of a scattering calculation where many configurations are the product of a target configuration with a continuum function. The new procedure, details of which are given in the Appendix, was found to be about 10 times faster than the previous one (Yoshimine, 1973). For example, a two-state run which comprised of 4864 uncontracted configuration spin functions (CSFs) took 43 Cray-YMP minutes to generate the symbolic matrix elements using the original algorithm, but only 5 minutes with the new.

Table 1. CO ($R = 2.132\ a_0$) vertical excitation energies compared with data given by Tilford and Simmonds (1972)

State	No of CSFs	Present CI target	Experiment
$a\,^3\Pi$	40	6.43	6.32
$A\,^1\Pi$	32	10.03	8.50
$a'\,^3\Sigma^+$	22	9.12	8.58
$d\,^3\Delta$	22	9.74	9.34
$e\,^3\Sigma^-$	25	10.19	9.86
$I\,^1\Sigma^-$	15	10.31	10.01
$D\,^1\Delta$	22	10.37	10.12

Table 2. Dipole and transition moments for selected states and geometries (compared with results of Peterson and Woods (1990) in brackets). All data in au.

R	$X\,^1\Sigma^+$	$a\,^3\Pi$	$a'\,^3\Sigma^+$	$a'-a$
1.9	−0.253 (-0.282)	0.318 (0.397)	−1.200 (-0.936)	0.467 (0.271)
2.0	−0.187 (-0.221)	0.377 (0.458)	−1.092 (-0.875)	0.401 (0.270)
2.13	−0.096 (-0.138)	0.419 (0.516)	−0.956 (-0.790)	0.351 (0.264)
2.5	0.151 (0.085)	0.405 (0.586)	−0.581 (-0.536)	0.237 (0.234)
2.8	0.346 (0.243)	0.512 (0.585)	−0.241 (-0.311)	0.164 (0.194)
3.0	0.499 (0.330)	0.660 (0.564)	0.047 (-0.168)	0.132 (0.165)

A requirement of our implementation of the multicentred R-matrix method is that it is necessary to use the same basic set of molecular orbitals in the construction of all target states. We used the STO basis given by Kirby-Docken and Liu (1977) to generate a total of

12σ, 8π, 6δ and 2ϕ molecular orbitals. The σ and π orbitals occupied in the ground $X\,^1\Sigma^+$ state and all of the δ and ϕ orbitals were obtained from an SCF calculation for the $X\,^1\Sigma^+$ state. The remaining σ and π orbitals were obtained from an SCF calculation for the lowest state of $^3\Pi$ symmetry. The CI target wavefunctions were constructed from the first 6σ and 2π orbitals using the complete active space of the 5σ, 6σ, 1π and 2π orbitals. It is clear that we could have generated better wavefunctions from this set of orbitals but this would have resulted in a very large number of terms to be included in the first term of equation (1). The vertical excitation energies that we obtained are compared with experiment in table 1. This also lists the number of CSFs used in the wavefunctions. The above prescription, which uses molecular orbitals from two different SCF calculations, has two advantages. The energy of the $^3\Pi$ state is much improved compared to that obtained using only ground state orbitals and the Schmidt orthogonalization of all orbitals of a given symmetry proved sufficient to ensure linear independence. The main disadvantage is that the energy of the $^1\Pi$ is quite poor. Another important criterion for selecting target states for use in scattering calculations is their ability to give accurate values for the various dipole and transition moments. In table 2 we compare values obtained from our adopted basis with those obtained from an elaborate CASSCF calculation by Peterson and Woods (1990). The overall level of agreement is quite satisfactory.

The errors in the vertical excitation energies were corrected by modifying the diagonal elements of the Hamiltonian matrix and shifting the threshold energies in the outer region. In order to avoid overcorrelating the CO^- states compared with the target states, we restricted the terms in the second expansion of equation (1) to those which correspond to the addition of one electron to configurations already included in the CI target wavefunctions. The Kirby-Docken and Liu (1977) basis contains some rather diffuse orbitals. We therefore checked that there were no spurious effects due to our finite R-matrix boundary. Our results were found to be quite insensitive to increasing the radius from our usual value of 10 a_0. Fixed nuclei calculations were carried out on a grid of 10 geometries, R = 1.8, 1.9, 2.0, 2.132, 2.25, 2.35, 2.5, 2.65, 2.8 and 3.0 a_0.

3. Results

We first checked that our current model could reproduce the low energy $^2\Pi$ resonance studied previously (Morgan 1991). In this earlier work we were unable to get good results when using a CI wavefunction for the ground state. This proved to be a consequence of the Lagrange orthogonalization procedure used to impose linear independence on the combined set of continuum and virtual orbitals. In the present calculation we used a different set of virtual orbitals which required less orthogonalization and therefore retained their original diffuse nature.

We carried out calculations for the overall symmetries $^2\Sigma^+$, $^2\Pi$, $^2\Delta$ and $^2\Phi$ and scattering energies in the range 6–18 eV. Resonances were observed in all symmetries. Their positions are shown in figure 2, together with the two lowest target states and the low-lying $^2\Pi$ resonance. The widths are shown in figure 3 (the low-lying $^2\Pi$ resonance, which is is much narrower and, at large bond lengths, becomes a bound state, is omitted and will not be discussed further in this paper). At any given geometry, the lowest $^2\Pi$ resonance has the smallest width and the highest has the largest. All of these new resonances are fairly broad and, with the exception of the lowest $^2\Pi$ and the $^2\Phi$, were difficult to locate at bond lengths of 2.1 a_0 and shorter. There are therefore significant uncertainties in the position and widths at these geometries. The situation is further complicated by the proximity of the

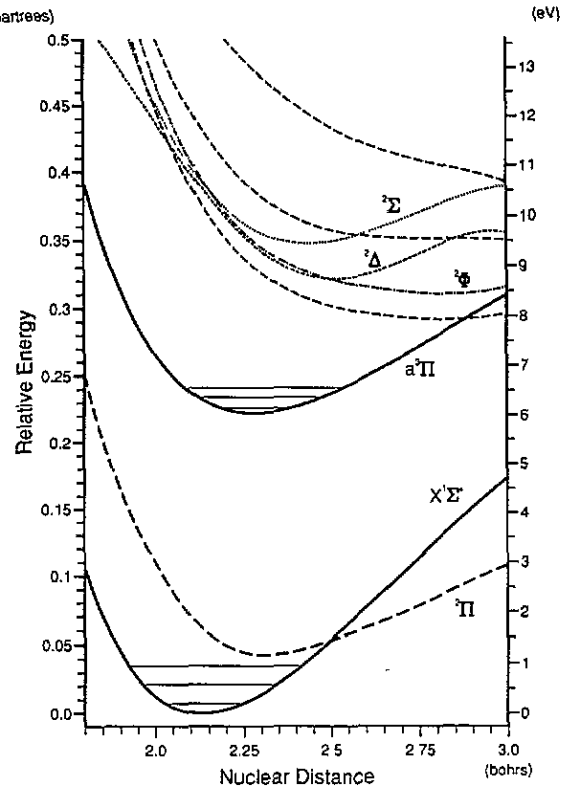

Figure 2. Resonance positions. Full curves, CO bound states; long-broken curves, $^2\Pi$ resonances; dotted curve, $^2\Sigma^+$ resonance; short-broken curve, $^2\Delta$ resonance; chain curve, $^2\Phi$ resonance.

excitation thresholds. At the equilibrium bond length of the ground state ($R = 2.132\ a_0$) the only resonances that we can fit with confidence are the $^2\Pi$ at 10.29 eV and the $^2\Phi$ at 10.81 eV. The situation improves at larger bond lengths but the large widths and the proximity of thresholds make it difficult to identify the parentage of most of the resonances. The lowest $^2\Pi$ and the $^2\Phi$ have very similar widths which could imply a common parent. The lowest state omitted from our model is the Rydberg b $^3\Sigma^+$ state which has its threshold at 10.66 eV at the equilibrium geometry of the ground state (see Tilford and Simmons 1972, figure 3). The omission of energetically allowed channels can give rise to spurious structure in the cross sections at energies above their thresholds. In the present calculations, this was only obviously apparent at scattering energies above 18 eV, hence we do not give results above this energy. Our highest $^2\Pi$ resonance, a very broad feature, could also be unphysical.

Cross sections were obtained at ten geometries and all four symmetries for the excitation of the seven excited states included in the model. At the equilibrium geometry of the ground state, the $^3\Pi$ state is well separated from the others and the fixed geometry calculation should be a good approximation to the excitation cross section summed over all vibrational levels. This transition has been studied by Sun *et al* (1992) using a three-state (X $^1\Sigma^+$, a $^3\Pi$ and A $^1\Pi$) model for energies from threshold to 30 eV and by Lee and McKoy (1982) using a two state model but only for energies of 20 eV and above. Experimental measurements have been carried out by Brongersma *et al* (1969), Ajello (1971), Swanson *et al* (1975), Allan

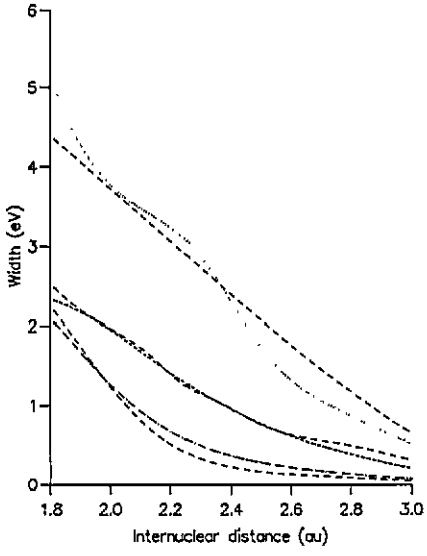

Figure 3. Resonance widths. Notation as in figure 2. The lowest $^2\Pi$ resonance is not shown.

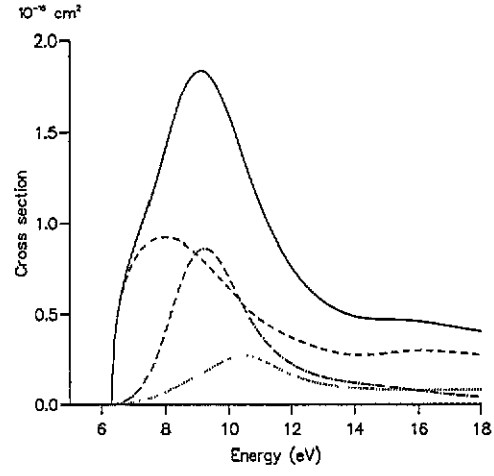

Figure 4. Cross section for the excitation of the a $^3\Pi$ state. Full curve, summed cross section; dotted curve $^2\Sigma^+$ contribution; long-broken curve, $^2\Pi$ contribution; chain curve, $^2\Delta$ contribution.

(1989) and Furlong and Newell (1993). Our cross sections, calculated at the equilibrium geometry of the ground state are shown in figure 4. The $^2\Delta$ resonance produces a peak in the cross section at about 9.5 eV. However, the largest contribution comes from the $^2\Pi$ symmetry. The broad hump is at too low an energy to be due to any of the three new $^2\Pi$ resonances found in the present calculations and appears, at the same position and magnitude, in simple two-state models. We therefore attribute it to the tail of the large $^2\Pi$ resonance at 1.8 eV. The $^2\Sigma$ contribution is much smaller but its resonance has a slight broadening effect on the summed cross section. The $^2\Phi$ contribution is negligible.

The early measurements by Brongersma *et al* (1969) and the vibrationally resolved excitation functions of Swanson *et al* (1975) both show sharply defined threshold peaks in the $^3\Pi$ cross section. None of the more recent experiments have confirmed this. If however such peaks do exist and are caused by some coupling of nuclear and electronic motion, such as the 'nuclear excited Feshbach resonances' seen in electron scattering by the hydrogen halides, then we would not see them either, since our fixed geometry model does not include any appropriate mechanism. Ajello's results have a similar shape to our own but the uncertainty in the magnitude of his cross sections may be as large as 75%. We compare our excitation cross section with the theoretical results of Sun *et al* and the experimental results of Furlong and Newell, and Allan in figure 5. Compared with the earlier theory, our peak is higher and occurs at a lower energy. The magnitudes at higher energies agree quite well. Neither experiment produced absolute cross sections. We have normalized the results of Furlong and Newell to give the same peak maximum as our own. Their results agree very well with ours up to the peak maximum; note that the apparent difference in excitation threshold is caused by our neglect of nuclear motion.

At higher energies the experimental data include some contribution from cascade and will therefore overestimate the true cross section. Allan's results are for the excitation of the $v = 0$ level only and are not absolute. However, there is no reason to suppose that the shape of the total cross section would be significantly different. We have arbitrarily

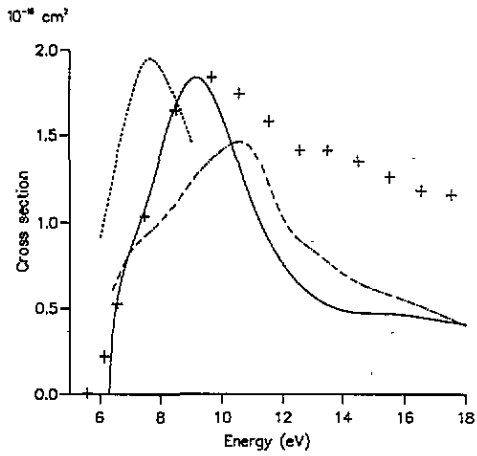

Figure 5. Cross section for the excitation of the a $^3\Pi$ state. Full curve, present results; chain curve, calculations of Sun *et al* (1992); crosses, measurements of Furlong and Newell (1993); short-broken curve, measurements of Allan (1989).

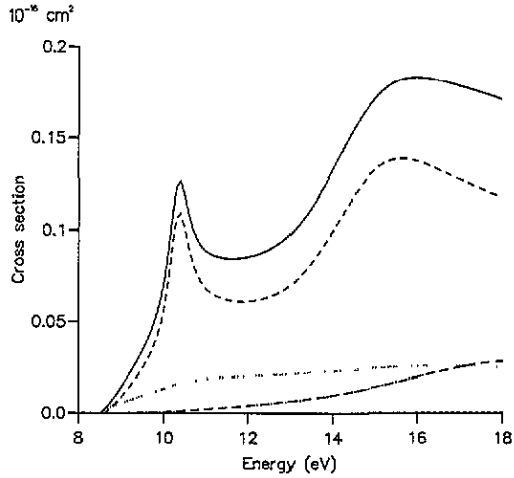

Figure 6. Cross section for the excitation of the a′ $^3\Sigma^+$ state. Notation as in figure 4.

normalized his results to have a peak maximum of 2×10^{-16} cm^2. This occurs at 7.5 eV, rather lower than our maximum at 9.1 eV.

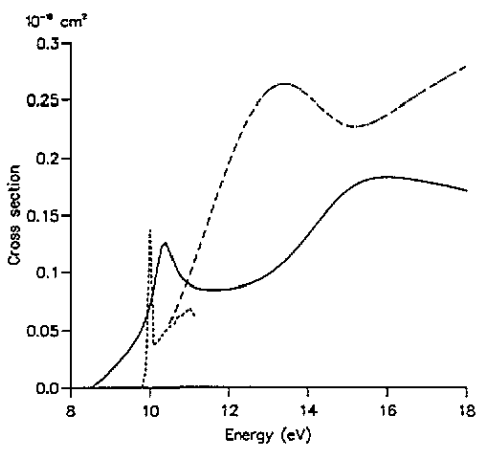

Figure 7. Cross section for the excitation of the a′ $^3\Sigma^+$ state. Notation as in figure 5.

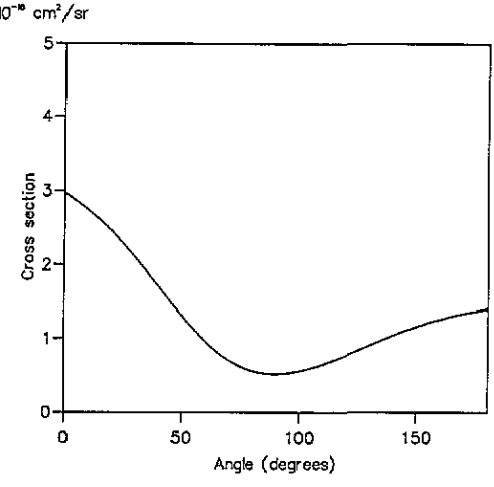

Figure 8. Differential cross section for the excitation of the a′ $^3\Sigma^+$ state at 10.4 eV.

The cross section for the excitation of the a′ $^3\Sigma^+$ state is shown in figures 6 and 7. We see a sharp resonance feature at 10.4 eV at the equilibrium geometry of the ground state. This correlates well with the structure seen in the measurements of Mazeau *et al* (1972) and most subsequent experimental work. It is not, however, apparent in the recent results of Sun *et al* ; they see a broader feature centred at 13.5 eV. Allan has also measured cross sections for the excitation of the $v = 3$ and $v = 27$ levels of the a′ $^3\Sigma^+$ state. The 10.04

eV resonance is only apparent in the latter. Mazeau *et al* have measured differential cross sections for several transitions. In particular, they have obtained data for the $v = 0$ and $v = 26$ levels. The latter are consistent with Allan's measurements, but the former, which cover the energy range 10–13 eV, show a lot of structure. Our results, which represent a vertical transition from the equilibrium geometry, are, due to Franck–Condon considerations, best compared with the high v transitions (see figure 1). In figure 7 we compare them, together with the results of Sun *et al* with Allan's data normalized to give good visual comparison. Our resonance, which is suffiently narrow and away from thresholds for us to be confident in its identification, has symmetry $^2\Pi$, not $^2\Sigma$ as the experimentally observed feature has been designated. This designation is based on the fact that the differential cross section in the vicinity of the peak is rather flat (Mazeau *et al* 1972), suggesting a dominant s-wave. They suggest that this resonance has parent states b $^3\Sigma^+$ and B $^1\Sigma^+$, neither of which are included in the present model. In contrast, our differential cross section at the peak maximum (figure 8) shows a predominantly p-wave behaviour, confirming that our resonance is not the feature seen in the experiments.

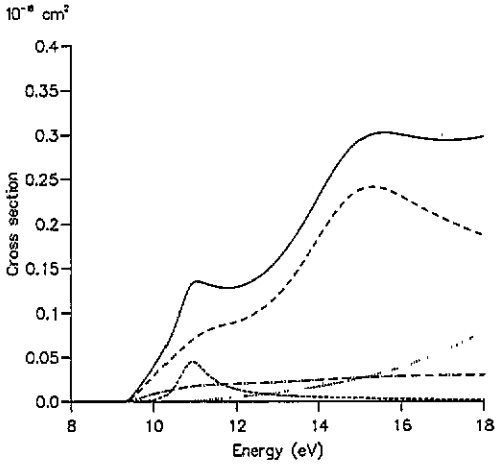

Figure 9. Cross section for the excitation of the d $^3\Delta$ state. Full curve, summed cross section; dotted curve $^2\Sigma^+$ contribution; long-broken curve, $^2\Pi$ contribution; chain curve, $^2\Delta$ contribution; short-broken curve, $^2\Phi$ contribution.

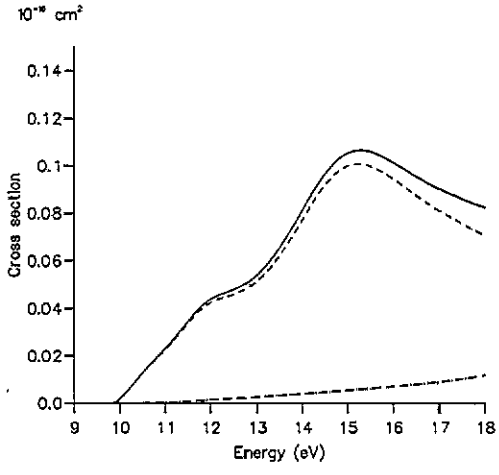

Figure 10. Cross section for the excitation of the e $^3\Sigma^-$ state. Notation as in figure 4.

Our cross sections for the excitation of the other metastable states are shown in figures 9, 10, 11 and 12. The d $^3\Delta$ results show a marked shoulder at about 11 eV due to the $^2\Phi$ resonance. The e $^3\Sigma^-$ cross section also has a shoulder at about 12 eV, but in this case it is due to a $^2\Pi$ resonance; in fact, the contribution from other symmetries is negligible in the energy range being considered. The I $^1\Sigma^-$ cross section is very similar, but is a factor of about 2.5 smaller. The D $^1\Delta$ cross section again has a similar shape and lies between the two Σ^- states in magnitude, but as in the case of the $^3\Delta$ cross section, the shoulder is due to the $^2\Phi$ resonance. In all four cases, the cross sections of Sun *et al* are significantly larger and show no structure.

We can compare our results with three experiments which have measured cross sections for the excitation of metastable states. Newman *et al* (1983) have measured cross sections for the excitation of all metastables in the energy range 6–16 eV. Their results are not

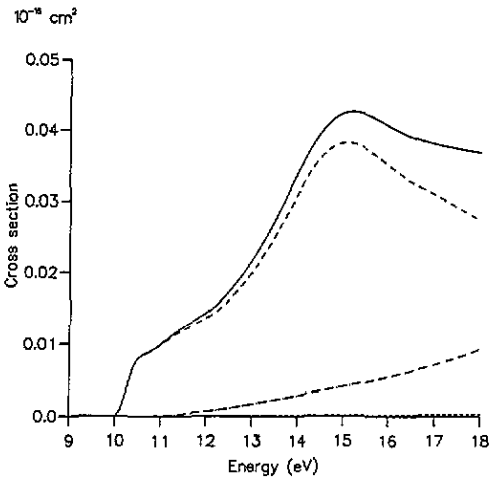

Figure 11. Cross section for the excitation of the $I\,^1\Sigma^-$ state. Notation as in figure 4.

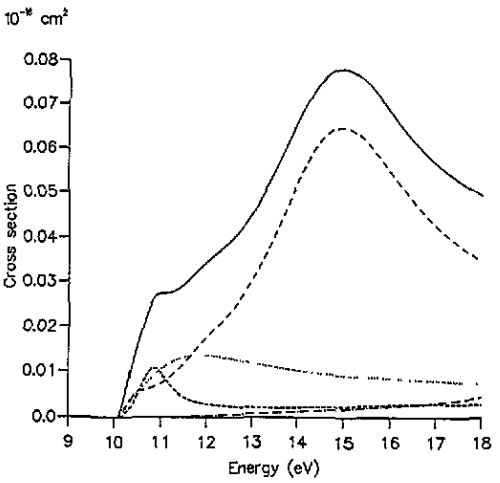

Figure 12. Cross section for the excitation of the $D\,^1\Delta$ state. Notation as in figure 9.

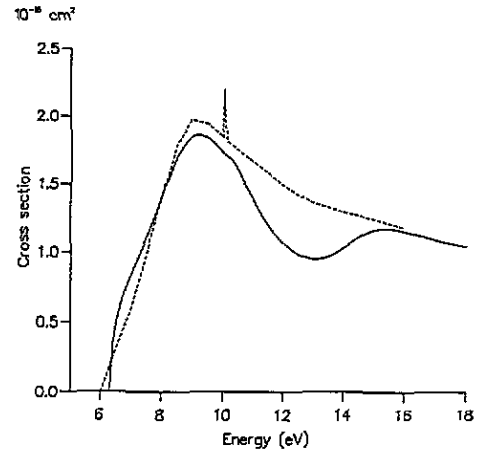

Figure 13. Cross section for the excitation of all metastable states. Full curve, present results; short-broken curve, measurements of Newman *et al* (1983).

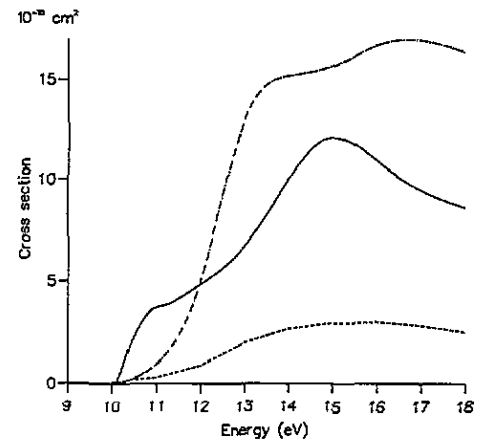

Figure 14. Cross section for the excitation of the higher metastable states. Full curve, present results; chain curve, calculations of Sun *et al* (1992); short-broken curve, measurements of Mason and Newell (1988).

normalized, so in order to compare with our present results we have arbitrarily normalized them so that the maximum of the broad peak is 2×10^{-16} cm^2. This is shown in figure 13. In our case, the a $^3\Pi$ cross section dominates so that the sharp peak in the a' $^3\Sigma$ is barely visible. We see a minimum in the cross section near 13 eV, but otherwise the shape is excellent agreement with experiment. Mason and Newell (1988) have measured cross sections for the excitation of the higher metastables $I\,^1\Sigma^-$ and $D\,^1\Delta$. Again theirs were relative measurements, but they normalized them to the results of Wells *et al* (1973). They are compared with our results in figure 14. Our cross section is about a factor of four greater than experiment, but has roughly the same shape. Sun *et al* also found a shoulder in their cross section but at a higher energy than the similar structure in our own. In our case it is due to a combination of the $^2\Pi$ resonance at 10.4 eV and the $^2\Phi$ at 11.3 eV.

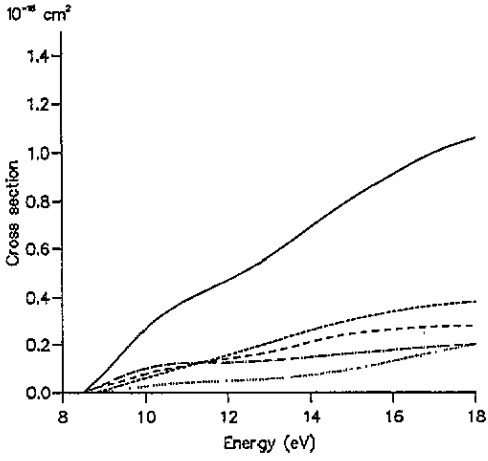

Figure 15. Cross section for the excitation of the A $^1\Pi$ state. Notation as in figure 9.

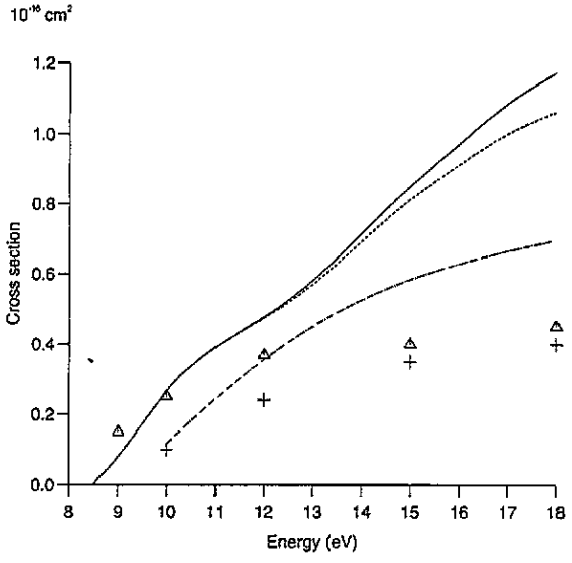

Figure 16. Cross section for the excitation of the A $^1\Pi$ state. Full curve, *R*-matrix results augmented by Born approximation; dotted curve, *R*-matrix results for first four symmetries only; chain curve, calculations of Sun *et al* (1992); triangles, experiment of Ajello (1971); crosses, experiment of Mumma *et al* (1971).

Finally our results for the excitation of the A $^1\Pi$ state are shown in figures 15 and 16. This is an optically allowed transition and it is clear that our results have not converged with respect to the sum over symmetries. Our original CI wavefunction was also poor and, although we corrected the vertical excitation energy (see table 1), we do not expect our results for this transition to be as reliable as the others. We have estimated the converged sum by adding contributions from higher symmetries (both m and l) obtained using the Born approximation. The resulting cross section is shown in figure 16 together with results of previous work. Our cross section lies considerably above that of Sun *et al* and the experimental measurements of Ajello (1971) and Mumma *et al* (1971).

4. Conclusions

We have identified six new resonances, three of symmetry $^2\Pi$ and one each of symmetry $^2\Sigma$, $^2\Delta$ and $^2\Phi$. However, at the equilibrium geometry of the ground state, only the lowest $^2\Pi$ is narrow enough to produce a distinct feature in the cross sections. There is an experimentally observed narrow resonance which has been designated $[CO^+ X^2\Sigma^+] (3s\sigma)^2 {}^2\Sigma^+$ with parents b $^3\Sigma^+$ and B $^1\Sigma^+$. Since neither of these states is explicitly included in our model, it is not surprising that we do not see it. We also find a $^2\Sigma$ resonance, at a slightly higher energy, but it is too broad to account for any observable structure. It could, however, be a poor representation of the observed resonance since the second term in equation (1) contains the appropriate configurations, though as pseudo-states whose energies are considerably higher than those of the physical states. Weatherford and Huo (1990) also looked for a CO^- state with configuration $[CO^+ X^2\Sigma^+] (3s\sigma)^2 {}^2\Sigma^+$. They found one at 11.044 eV, 1 eV higher than experiment. They attribute this to their failure to include sufficient correlation in their CO^+ grandparent state. Their calculation was only at SCF level. Our CI calculation, though restricted, should be significantly better, but only produces a 0.3 eV shift, to 10.7 eV. Weatherford and Huo also failed to find any Feshbach resonances below the b $^3\Sigma^+$ threshold.

Our results are generally in good agreement with the overall shapes of the various experimental integrated cross sections. As noted above, none of the recent work has obtained absolute cross sections and, where normalization has been attempted using older data, this results in magnitudes rather smaller than our present results. We do not agree so well with the shapes of the cross sections calculated in the recent work of Sun *et al* (1992), though we broadly agree with their magnitudes.

The present model does not include nuclear motion. Previous work, where it has been included (Morgan 1991, Mündel *et al* 1985) suggests that broad resonances, such as those found here, will be relatively unaffected. There is no reason to suppose that there will be significant non-adiabatic effects in the energy range under consideration. However, the inclusion of nuclear motion using a non-adiabatic treatment (Schneider *et al* 1979) is feasible and will form the next phase of this work.

Acknowledgments

We thank Charles Gillan and Joan Furlong for helpful discussions during the course of the work and SERC for support under grant GR/H41744.

Appendix. Prototype treatment of symbolic matrix elements

Our molecular R-matrix code is based on the quantum chemistry code ALCHEMY (McLean 1971) which uses a traditional treatment of the configuration interaction (CI) problem. The program generates configuration spin functions (CSFs), computes symbolic matrix elements for the lower triangle of the Hamiltonian matrix in terms of integral lists, sorts the elements into a canonical order and finally use this sorted list to explicitly construct the CI Hamiltonian matrix (Yoshimine 1973). Although such methods have been superseded in present state-of-art electronic structure packages, they have features for scattering calculations which are hard to reproduce with more group theoretical methods.

In our R-matrix scattering calculations it is necessary to tightly control the model being used: N electron as well $N + 1$ electron coupling constraints must be enforced so that

target states can be identified on the R-matrix boundary; the (L^2) configurations used to represent polarization and correlation effects must be carefully selected so that the correct balance between target (N electron) and scattering ($N+1$ electron) problems is obtained; in a CI target calculation, care must also be taken that the configurations in the N and $N+1$ electron calculations have the same phase (Noble 1992). These can all be accomplished with adaptations of the procedure outlined above.

However the generation of symbolic matrix elements in this traditional method is inefficient and can easily become a constraint on the size of calculation attempted. This is particularly true for CI target calculations where the number of CSFs generated is the number of continuum functions *times* the number of CI target CSFs summed over each target state in the scattering calculation, plus the number of correlation and polarization CSFs. It is this problem that has limited previous molecular R-matrix calculations to target wavefunctions with 30 or less configurations.

An adaptation of the prototype CI method originally introduced by Liu and Yoshimine (1981) and further developed by Liu and Lengsfield (1991) offers a way out of this problem. These workers recognised that many symbolic matrix elements were composed of the same symbolic integrals which differed merely in their indices in some systematic way. In our scattering calculations this feature is particularly apparent as each target CSF is coupled to between 20 and 50 continuum functions of the appropriate symmetry. Furthermore, the nature of low-energy scattering means that no more than one electron is ever in a continuum orbital in *any* configuration; those with no electrons in a continuum orbital being referred to as 'L^2' and denoted by ℓ below.

In the method presented here only symbolic matrix elements involving the first two continuum functions for each target configuration and continuum symmetry are explicitly evaluated, the remaining matrix elements being constructed from these as described below. Matrix elements involving two continuum functions are evaluated as this allows for the calculation of a prototypical off-diagonal symbolic matrix element, as well as, of course two diagonal ones. By convention CSFs contributing to a particular target state are generated together and 'L^2' CSFs are generated last. This convention is also adopted in our programs which contract CI target wavefunctions, details of which have been given elsewhere (Branchett 1991).

Consider a general prototype matrix element $\langle C(i, j^{\Gamma})|H|C'(i', j'^{\Gamma'})\rangle$, where CSF C comprises the suitably coupled product of target CSF i and continuum orbital j with symmetry Γ. In C, the first continuum orbital of given symmetry is denoted by $j^{\Gamma} = a$, the second by $j^{\Gamma} = b$ and L^2 CSFs by $j^{\Gamma} = \ell$. Each prototype symbolic matrix elements matrix element is read and processed as follows.

(i) Diagonal element ($C = C'$)?

(a) If $j = a$ or ℓ: copy matrix element.

(b) If $j = b$: expand along the diagonal.

(ii) Off-diagonal element with L^2 CSF ($j' = \ell$)?

(a) If $j = a$ or $j = \ell$: copy matrix element.

(b) If $j = b$: expand along the row.

(iii) Off-diagonal element with same target CSF and same continuum symmetry ($\Gamma = \Gamma', i = i'$)?

Expand into an off-diagonal lower triangle.

(iv) Continuum symmetry same, but target CSFs different ($\Gamma = \Gamma', i \neq i'$)?

(a) First 'diagonal' element ($j = j' = a$): expand along the diagonal.

(b) Lower triangle 'off-diagonal' element ($j = a, j' = b$):

Expand into an off-diagonal lower triangle.

(c) Upper triangle 'off-diagonal element' ($j = b$, $j' = a$):
Expand into an off-diagonal upper triangle.
(d) Second 'diagonal' element ($j = j' = b$): skip.
(v) Continuum symmetries different ($\Gamma \neq \Gamma'$)?
(a) First occurrence ($j = a$, $j' = a'$): expand into rectangular block.
(b) Other elements: skip.

The expansions thus can be broken up into five basic types: along a diagonal, down a column, lower triangle, upper triangle and rectangular block. Each expansion type has been coded as a fairly simple subroutine. This procedure actually produces matrix elements in a different order to the one in use previously, but this only required relatively minor modification to the routines which explicitly construct the Hamiltonian matrix.

References

Ajello J M 1971 *J. Chem. Phys.* **55** 3158
Allan M 1989 *J. Electron. Spectrosc. Rel. Phenom.* **48** 219
Branchett S E 1991 *PhD Thesis* University of London
Branchett S E, Tennyson J and Morgan L A 1990 *J. Phys. B: At. Mol. Opt. Phys.* **23** 4625
Brongersma H H, Boerboom A J H and Kistemaker J 1969 *Physica* **44** 419
Furlong J and Newell W R 1993 *Proc. 18th Int. Conf. on Physics of Electronic and Atomic Collisions* (Bristol: IOP) Abstracts
Gillan C J, Nagy O, Burke P G, Morgan L A and Noble C J 1987 *J. Phys. B: At. Mol. Phys.* **20** 4585–603
Gillan C J, Noble C J and Burke P G 1990 *J. Phys. B: At. Mol. Opt. Phys.* **23** L407
Kirby-Docken K and Liu B 1977 *J. Chem. Phys.* **66** 4309
Land J E 1978 *J. Appl. Phys.* **49** 5716
Lee M and McKoy V 1982 *J. Phys. B: At. Mol. Phys.* **15** 3971
Liu B and Lengsfield B H 1991 *Modern Techniques in Computational Chemistry: MOTECC-91* ed E Clementi (Leiden: Escom) ch 6B
Liu B and Yoshimine M 1981 *J. Chem. Phys.* **74** 612
Mason N J and Newell W R 1988 *J. Phys. B: At. Mol. Opt. Phys.* **21** 1293
Mazeau J, Gresteau F, Joyez G, Reinhardt J and Hall R I 1972 *J. Phys. B: At. Mol. Phys.* **5** 1890
McDaniel E W and Nigham W L 1982 *Appl. At. Collision Phys.* **3** 294
McLean A D 1971 *Conf. Potential Energy Surfaces in Chemistry* ed W A Lester Jr (San Jose: IBM Research Laboratory) p 87
Morgan L A 1990 *Proc. 16th Int. Conf. on Physics of Electronic and Atomic Collisions* ed A Dalgarno, R S Freund M S Lubell and T B Lucatorto (New York: Plenum) Invited Papers and Progress Reports pp 96–102
—— 1991 *J. Phys. B: At. Mol. Opt. Phys.* **24** 4649
Mumma M J, Stone E J and Zipf E C 1971 *J. Chem. Phys.* **54** 2627
Mündel C, Berman M and Domcke W 1985 *Phys. Rev.* A **32** 181
Newman D S, Zubek M and King G C 1983 *J. Phys. B: At. Mol. Phys.* **16** 2247
Noble C J 1992 Private communication
Noble C J and Burke P G 1992 *Phys. Rev. Lett.* **68** 2011
Peterson K A and Woods R C 1990 *J. Chem. Phys.* **93** 5029
Sarpal B K, Tennyson J and Morgan L A 1991 *J. Phys. B: At. Mol. Opt. Phys.* **24** 1851
Schneider B I, Le Dourneuf M and Burke P G 1979 *J. Phys. B: At. Mol. Phys.* **12** L365–9
Sun Q, Winstead C and McKoy V 1992 *Phys. Rev.* A **46** 6987
Swanson N, Celotta R J, Kuyatt C E and Cooper J W 1975 *J. Chem. Phys.* **62** 4880
Tilford S G and Simmons J D 1972 *J. Phys. Chem. Ref. Data* **1** 147
Weatherford C A and Huo W M 1990 *Phys. Rev.* A **41** 186
Wells W C, Borst W L and Zipf E C 1973 *Phys. Rev.* A **8** 2463
Urban W 1991 *Laser Optoelectron.* **23** 56
Yoshimine M 1973 *J. Comput. Phys.* **11** 333